Optical Materials EXPRESS

Photonic neuromorphic computing using vertical cavity semiconductor lasers

ANAS SKALLI,[1,*] JOSHUA ROBERTSON,[2] DAFYDD OWEN-NEWNS,[2] MATEJ HEJDA,[2] XAVIER PORTE,[1] STEPHAN REITZENSTEIN,[3] ANTONIO HURTADO,[2] AND DANIEL BRUNNER[1]

[1]*Institut FEMTO-ST, Université Bourgogne Franche-Comté CNRS UMR 6174, Besançon, France*
[2]*Institute of Photonics, SUPA Department of Physics, University of Strathclyde, Glasgow, United Kingdom*
[3]*Technical University of Berlin/Institute of Solid-State Physics and the Center of Nanophotonics, Hardenbergstraße 36, D- 10632 Berlin, Germany*
[*]anas.skalli@femto-st.fr

Abstract: Photonic realizations of neural network computing hardware are a promising approach to enable future scalability of neuromorphic computing. The number of special purpose neuromorphic hardware and neuromorphic photonics has accelerated on such a scale that one can now speak of a Cambrian explosion. Work along these lines includes (i) high performance hardware for artificial neurons, (ii) the efficient and scalable implementation of a neural network's connections, and (iii) strategies to adjust network connections during the learning phase. In this review we provide an overview on vertical-cavity surface-emitting lasers (VCSELs) and how these high-performance electro-optical components either implement or are combined with additional photonic hardware to demonstrate points (i-iii). In the neurmorphic photonics context, VCSELs are of exceptional interest as they are compatible with CMOS fabrication, readily achieve 30% wall-plug efficiency, >30 GHz modulation bandwidth and multiply and accumulate operations at sub-fJ energy. They hence are highly energy efficient and ultra-fast. Crucially, they react nonlinearly to optical injection as well as to electrical modulation, making them highly suitable as all-optical as well as electro-optical photonic neurons. Their optical cavities are wavelength-limited, and standard semiconductor growth and lithography enables non-classical cavity configurations and geometries. This enables excitable VCSELs (i.e. spiking VCSELs) to finely control their temporal and spatial coherence, to unlock terahertz bandwidths through spin-flip effects, and even to leverage cavity quantum electrodynamics to further boost their efficiency. Finally, as VCSEL arrays they are compatible with standard 2D photonic integration, but their emission vertical to the substrate makes them ideally suited for scalable integrated networks leveraging 3D photonic waveguides. Here, we discuss the implementation of spatially as well as temporally multiplexed VCSEL neural networks and reservoirs, computation on the basis of excitable VCSELs as photonic spiking neurons, as well as concepts and advances in the fabrication of VCSELs and microlasers. Finally, we provide an outlook and a roadmap identifying future possibilities and some crucial milestones for the field.

1. Introduction

Neural networks (NN) are concepts fundamentally relying on a *connectionist* approach to computation, a concept that was developed based on the most-simplified features of a biological neuron, see Fig. 1(a). In a biological neuron, an axon typically forms a long-range link that connects via synapses to the dendrites of the post-synaptic neuron. Furthermore, a neuron's inner working principles makes them respond nonlinearly to inputs. Following this principle, a NN creates and combines a large number of simple nonlinear transformations by artificial neurons, or perceptrons, while a training phase tweaks the network's topology such that specific computations result from emergence. This enables computing outside the classical symbolic programming and

Boolean logic-gates catalogue: programming is replaced by statistical NN-topology optimization, while the hardware-concept is based on networks of simple nonlinear units rather than on mostly serial threads of logic gates with fixed and premeditated topology. The increased flexibility in programming a computer enables addressing highly abstract computational challenges, and NNs currently drive a revolution in various areas of economy, technology and society. However, in a NN concept, all artificial neurons simultaneously express their transformations of input signals, which intimately links NNs to parallelism.
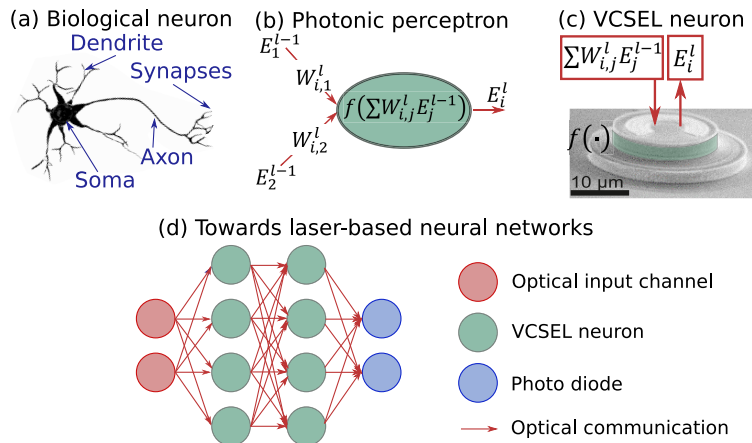

Fig. 1. (a) Biological neurons form complex connections using synapses, which link axons and dendrites of pre- and post-synaptic neurons. Crucial for computation is their nonlinearity. (b) The optical perceptron mimics this functionality by nonlinearly transforming a sum of optical fields from neurons in layer l E_j^{l-1}, scaled by connection weights W_j^l, to the neuron's output field E_i^l. (c) VCSELs can efficiently be coupled to external fields, and their internal workings make them respond nonlinearly to such optical injection. (d) Linked via photonic connections, VCSELs offer a promising roadmap to photonc neural networks.

Today's computing substrates can follow the connectionist principle only within tight limits, and the development of scalable, efficient, high performance hardware NNs currently is a major goal. The principle operations are information transformation, information transduction across the network, and topology optimization. Leveraging photons is highly promising for implementing parallel NN interconnects [1] and in particular in combination with photonic NN (PNN) computing [2,3]. In a photonic perceptron, see Fig. 1(b), optical inputs from the network are accumulated and nonlinearly transformed. Optical communication is inherently parallel [4], energy efficient [5] and recent developments in optical memristors indicate a roadmap towards programmability [6].

However, competitive nonlinear photonic components for artificial neurons have been a challenge. Lately, the energy consumption of novel photonic devices is approaching that of their electronic counterpart [7], and a general strategy to enhance nonlinearity is to confine photons into a tight space or to increase the interaction time, often by using optical resonators such as the case for lasers. Vertical-cavity surface-emitting lasers (VCSELs) are one of the most prominent semiconductor lasers, with unique properties making them highly suitable for next generation PNN hardware. Figure 1(c) illustrates a VCSEL after fabrication and highlights how a VCSEL-based neuron would receive, transform and send information. VCSELs profit from high-yield commercially mature fabrication, readily reaching above 30% wall-plug efficiency [8]. Furthermore, due to their low lasing threshold currents and amplitude-phase coupling via Henry's alpha factor, they react highly nonlinear to optical input and can therefore act as all-optical as

well as electro-optical artificial neurons. VCSELs can readily be modulated with >30 GHz [8]. Such high efficiency and high speed combined result in an ultra low energy per nonlinear transformation on the order of 10 fJ [9]. Considering the parallelism of a potentially passive and low-loss massive interconnect comprising $>10^2$ connections per channel, this brings PNNs using VCSELs into the realm of <100 aJ per Operation, compared to 100 fJ...1 pJ in electronic circuits. Crucially, this is only a current snapshot, and spin-VCSELs [10], high-β VCSELs leveraging cavity quantum electrodynamics as well as nanolasers [11] can further reduce this cost towards the fundamental physical limits on the order of a few photons per operation [12].

VCSELs emit vertically to their substrates, which allows for efficient testing and for interfacing with scalable 3D integrated photonic circuits [13] or external optical resonators [14] in order to establish a PNN's connections, see Fig. 1(d). Furthermore, in order to realize numerous photonic neurons they can be arranged in arrays [9], or, as recently demonstrated, one can leverage spatial multiplexing of a multimode large area VCSEL in order to implement photonic neurons in spatial modes [15]. An additional concept to extend the number of degrees of freedom are the two orthogonal polarization directions [16]. Finally, VCSEL structures can be operated in an excitable regime, either relying on intra-cavity saturable absorbers [17] or on injection-locked induced excitability [18].

Owing to such promising properties, semiconductor laser-based PNNs have a long standing history [19]. Initially, the difficulties in training and implementing large NN limited the field's progress. With the introduction of reservoir computing (RC) [20] this challenge was efficiently mitigated, and in combination with a temporal-multiplexing approach [21] large-scale PNNs could be successfully emulated [22].

In this review, we provide a detailed overview on the implementation of VCSELs in different PNN topologies, different VCSEL-based photonic neuron concepts as well as cutting edge VCSEL fabrication. In Sec. 3 we discuss the temporal-multiplexing approach for PNNs, in Sec. 4 the implementation of PNNs in spatially extended multimode lasers, while excitable photonic spiking VCSEL neurons are discussed in Sec. 5, the fabrication of modern VCSELs structures in Sec. 6. At the end of our review we provide an extensive outlook in Sec. 7, which includes a roadmap to guide the field's future development.

2. Principles of a VCSEL

Photonic hardware provides neuromorphic computing with low-loss optical interconnects, intrinsic non-linearity and ultrafast operation rates [5]. Suitable devices include optical modulators and different semiconductor lasers such as edge-emitting lasers, resonant tunnelling diode-laser-diode systems and VCSELs [23,24]. The latter are of particular interest because of their commercial availability, their compactness (in comparison to edge-emitters) and their vertical emission with close-to-ideal Gaussian emission profiles.

VCSELs can have many different configurations, yet they all feature identical design principles. Horizontally arranged high-reflectivity dielectric mirrors sandwich a gain material inside the cavity formed between the two mirrors. Often, this cavity is very short and only half a wavelength long. These planar structures are then etched to form pillars, or mesas, and optical emission is through the top-mirror that typically features a slightly lower reflectivity (between ~99.0% and ~99.8%). A schematic illustration of this principle is given in Fig. 2, and details of semiconductor VCSEL growth can be found in Sec. 6. Mirrors are usually distributed Bragg reflectors (DBRs), comprising layers of different semiconductor materials transparent at the lasing wavelength yet with different refractive indices, while optical gain can either be realized using one or more quantum wells or ensembles of quantum dots.

The dynamics of VCSELs are usually described using rate equation models. Compared to standard edge emitting semiconductor lasers, VCSELs do however require a more complex description, as they can commonly emit in and hence require modeling of orthogonal optical
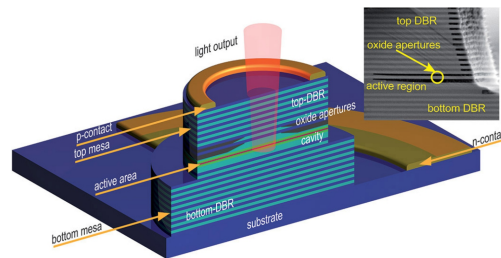
Fig. 2. Schematic representation of a VCSEL device. The compact, vertical emitting laser consist essentially of two doped DBRs, a central cavity with the active area, at least one oxide aperture, and ring-shaped n- and p-contacts. Inset: Scanning electron microscope image showing the central area (cross-section) of a VCSEL with two oxide apertures. Reproduced with permission from Ref. [25]

polarizations and the associated carrier spin-populations. The standard set of equations is based on the spin-flip model [26]. These features make their numerical description more complex, but this complexity is an asset for computation and allows for higher dimensionality or complexity of VCSEL-neurons and excitable behaviour, see Sect. 5.

An important parameter is the carrier's relaxation oscillation frequency, whose usual timescale of 0.1...10 GHz typically determines the bandwidth of a VCSEL's nonlinear transformation. Furthermore, if information is to be injected optically, then the usually 1...5 ps lifetime of a photon within the VCSEL's cavity is important. Optical information injection requires locking the VCSEL serving as photonic perceptron to an external injection laser [27]. Such optical injection locking can only be realized inside a narrow range of frequency detuning between injection and response laser. The width of this detuning window is determined by the ratio of injection and the VCSEL's emission power, and the VCSEL's photon lifetime acts as a scaling factor: the longer the lifetime, the more frequency selective the VCSEL, and consequently the narrower the injection locking window is for a given power ratio.

3. Time delayed reservoirs

The concept of delay-based reservoir computing was first introduced in the seminal paper of Appeltant et al. [21]. Mathematically, delay systems are described by delay differential equations whose temporal solution depends on the present as well as on past states. As such, when delayed feedback is added, even a low-dimensional system offers the high-dimensional phase space that forms the basis for RC. In contrast to spatially-extended RC systems, this approach uses only a single nonlinear node and a linear delayed feedback line with round trip duration τ, as illustrated in Fig. 3(a). The nonlinear node continuously transforms the information fed back from the delay line. A number of virtual nodes (or virtual neurons) are then created by discretizing the continuous output of the delayed system in N time segments of length θ, often fulfilling the relation $N = \tau/\theta$. Delay RC process input information $I(t)$ sequentially and their operation speed is determined by the long delay length τ: each input sample is mapped onto the complete set of virtual nodes N and multiplied by a random mask $m(t)$ with periodicity τ. This temporal mask is introduced to diversify the response of the virtual nodes to the input signal and plays a similar role as the input weights in a conventional reservoir. Inertia [21] or de-synchronization between injection mask length and delay τ [28] realize the reservoir's internal connections. Typically, the input masking and the output layer weights are implemented off-line with a digital computer. The values $y_{out}(t)$ (cf. Figure 3(a)) are obtained one at a time in intervals of τ from the continuous analogue output, and they are calculated as a linear combination of the θ-spaced states of the

virtual nodes, creating reservoir state x(t). The samples are then concatenated to state matrix *S* where columns represent time and rows represent the neurons.
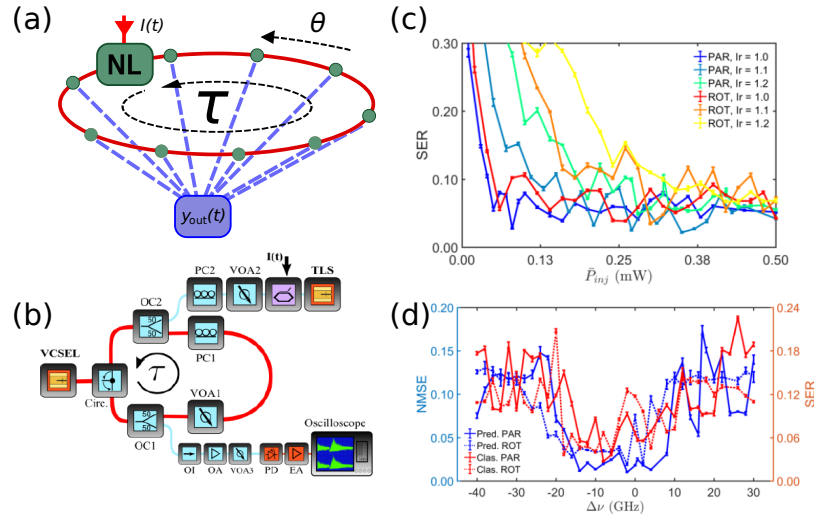

Fig. 3. (a) Delay-based reservoir computing. (b) Scheme of the experimental setup for a VCSEL delay-based reservoir computer. OC: Optical Coupler, PC: Polarization Controller, VOA: Variable Optical Attenuator, TLS: Tunable Laser Source, PD: Photodiode, EA: Electrical Amplifier, OI: Optical Isolator. (c) Performance of a VCSEL delay RC on a classification task as a function of the average optical injected power for parallel (PAR) and rotated (ROT) feedback [29]. (d) Performance of the same VCSEL RC on prediction (Pred.) and classification (Clas.) tasks for PAR and ROT feedback as a function of the frequency detuning [29]. (b)-(d) © 2022 IEEE. Reprinted, with permission, from [29].

Delay-based RC aims at mitigating hardware complexity of spatially-extended systems using a single nonlinear node only, a delay line and high-bandwidth capabilities for injection and detection. When implemented in photonics, delay-based RC systems have successfully been employed for classification, prediction and system-modelling tasks with state-of-the-art results. The specific motivation for photonic delayed RC implementations is the availability of off-the-shelf fiber-optics telecommunications hardware and that the physical length of the delay line does not impact the modulation bandwidth θ^{-1}, cf. Figure 3(b). The first optical hardware implementations of RC were independently developed by Larger et al. [30] and Paquot et al. [28] using optoelectronic systems. Soon after, the first implementation with a semiconductor laser showed excellent performance for RC at Gbyte/s rates [31], the system's injection locking parameter space was investigated in [27].

Implementations involving VCSELs leverage their polarization properties to improve the information processing performance and speed. Typically, one of the two optical modes dominates, but their relative intensities change depending on laser, optical feedback and injection parameters. Time delayed RC based on VCSELs explore polarization dependencies to build alternative feedback schemes by rotating the polarization of the feedback or even exploring dual processing by simultaneously computing with the two modes. Vatin et al. numerically [32] and experimentally [16] first demonstrated delay-based RC with two-mode polarization dynamics of a VCSEL. Using either parallel (PAR) or orthogonal (ROT) configurations, a comprehensive experimental analysis can be found in [29], where the authors analyze the performance of both feedback configurations with Mackey-Glass prediction and nonlinear channel equalization tasks, see Fig. 3(c,d). The authors find that ROT feedback degrades the computational performance in

terms of memory capacity when there is a significant power difference between the two emission modes [29].

Dual emission also offers the possibility of implementing two tasks in parallel, where each task is performed by one of the two perpendicularly polarized modes. This was first proposed numerically in [33] and later on demonstrated experimentally in [34]. Dual task operation slightly degrades the system's performance for each task, but nevertheless represents an attractive advantage of VCSELs. Finally, Harkhoe et al. [35] proposed and numerically investigated the use of fast spin-flip dynamics in VCSELs to boost the information processing speed at multi-GSa/s. The speed of the spin-flip dynamics, which depend on the birrefringence of the VCSEL, can further be increased by more than one order of magnitude [10].

Delay-based reservoirs enable minimal hardware requirements [22], yet information is still processed sequentially, requiring complex time multiplexing, while computational speed still depends on the size of a time-multiplexed PNN layer. It also entails that most implementations still rely on an external computer to pre-process data, construct the reservoir state and calculate the output weights for training. In [36], an online learning strategy is implemented to reduce the influence of the external computer. However, the sequential nature remains a fundamental feature (and asset) of this system.

4. Spatio-temporal reservoirs

Using large area VCSELs (LA-VCSELs), e.g. with an aperture of 25 μm and leveraging their highly multimode nature, a truly parallel, spatially multiplexed, VCSEL-based reservoir was introduced in [15]. Due to parallelism, computing speed does in this system not depend on the PNN's size any longer. In addition, an online learning strategy was implemented, making the system's computation fully autonomous and relegating the external computer to a simple supervision and instrument-control role.

4.1. Working principle and experimental setup

The PNN implemented in [15] can be broken up into three functional sections, c.f. Figure 4(a). First, the input layer is realised via a digital micromirror device (DMD_a) and a multimode fibre (mmf). Spatial patterns (Boolean images) displayed on DMD_a constitute the input information, **u** in Fig. 4(a), and the mmf passively implements the PNN's input weights via its complex transmission matrix.

The second part is the reservoir itself. The output field of the mmf is optically injected via imaging onto the LA-VCSEL top-facet, which implements all the components of the reservoir through its spatio-temporal nonlinear dynamics. Nodes are spatially multiplexed positions on the LA-VCSEL's surface, and coupling is taken care of by carrier diffusion and optical diffraction inside the LA-VCSEL's cavity. The reservoir state is then the perturbed mode-profile of the LA-VCSEL under optical injection, denoted in Fig. 4(a) as **x**. In Fig. 4(b), the VCSEL's response is shown for several 3-bit headers. Responses to each input pattern are complex and different. This explains, in an intuitive sense, how finding a configuration of output weights that solve a certain computational task like header recognition, XOR, and digital-analog conversion [15] is possible. Ultimately, the reservoir is used at speeds orders of magnitudes below its inherent timescales, and the LA-VCSEL was operated in its steady state, hence no recurrent properties such as fading memory of the device were exploited. In order to use the concept presented here for memory dependant tasks such as time series prediction, one would have to encode the input information on the timescale of the VCSEL's intrinsic dynamics by using for instance, a gigahertz-rate modulator.

The last part of this PNN is its output layer with weights $\mathbf{W}^{out}$, which are realized by imaging the LA-VCSEL's near field onto a second DMD (DMD_b). The reflection off DMD_b in one direction is imaged onto a large area detector, and the mirrors of DMD_b sample the different
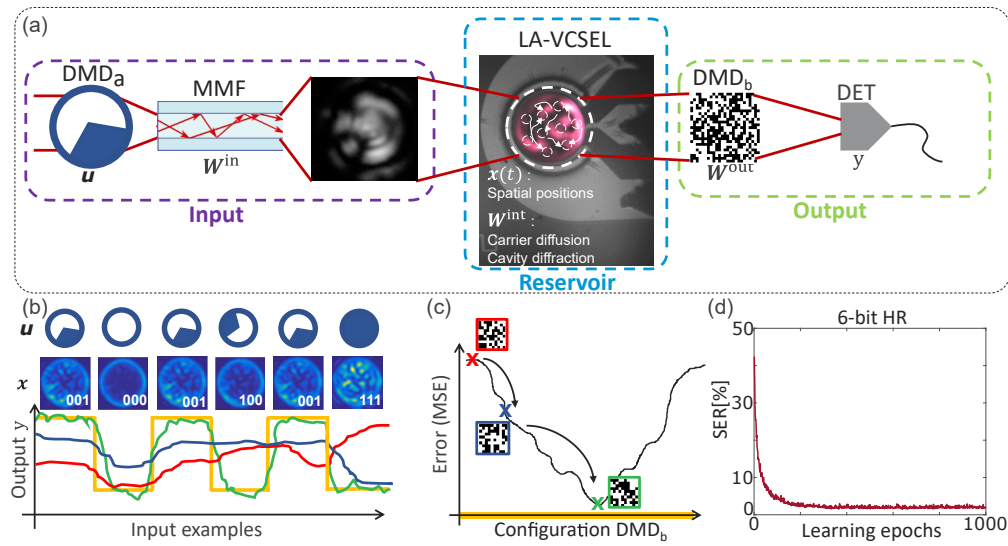
Fig. 4. (a) Working Principle of the LA-VCSEL spatially multiplexed reservoir. (b) Input information **u** and the LA-VCSEL response for 3-bit binary headers. The graph shows the target output y^{target} and different reservoir outputs y^{out} of decreasing mean square error (MSE) (red, blue and green). (c) Schematic illustration of the error landscape, showing the MSE as a function of the output weights configuration. The outlined (red, blue and green) Boolean matrices correspond to the output weights giving the output from b). (d) Representative performance of the PNN on a 6bit header recognition (HR) task. Reproduced with permission from [37].

positions, i.e. neurons on the LA-VCSEL's surface. This applies a Boolean weight matrix to the reservoir state, and the authors implemented ~90 trainable Boolean readout weights. The output of the network y^{out} was recorded at the detector for a set of input patterns called the training batch. For each image t in the training batch, the desired target output $y^{\text{target}}(t)$ is known. Thus, after each training epoch (a run of one batch), y^{out} is recorded and a normalized mean square error is calculated $\epsilon_k = ||y_k^{\text{out}}(t) - y^{\text{target}}(t)||$. Training is realised via a simple, yet effective evolutionary algorithm presented in [38,39]. Boolean weights (mirrors) at random positions are flipped at the transition from k to $k + 1$. If the change is beneficial, i.e. $\epsilon_{k+1} < \epsilon_k$, it is kept, otherwise the output weights are reset to the configuration at epoch k as shown in Fig. 4(b,c). This operation is repeated until the desired performance threshold is met. Figure 4(d) shows a representative learning curve for a 6bit header recognition task, for which the system reaches around a 1.5% symbol error rate (SER).

4.2. LA-VCSEL PNN metrics

The performance of the LA-VCSEL reservoir is extensively studied in [37], mapping the impact of several parameters on the overall performance. Figure 5(a) shows how the LA-VCSEL's free running modes react to external optical injection. At $\lambda_{\text{inj}} = 918.9$ nm, a resonance condition is met where the LA-VCSEL's free running modes are suppressed (by ≈ 10 dB) and the device locks to the injection laser, that is to say, the VCSEL's emission wavelength is shifted to that of the external drive laser. Injection locking has been extensively studied in [40,41]. In Fig. 5(b), we see a clear dependence of the performance on the injection wavelength as well as the injection power ratio (PR = $P_{\text{inj}}/P_{\text{VCSEL}}$), and the best performance is obtained under locking, consistent with [27] for a semiconductor laser delay reservoir.
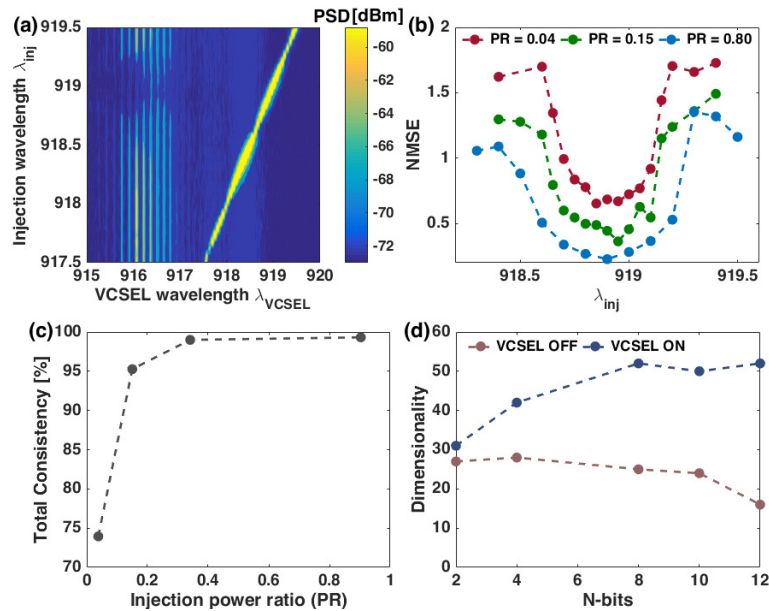
Fig. 5. (a) Injection locking of the VCSEL by an external drive laser. (b) Performance (NMSE) vs Injection wavelength for different injection power ratios (PR), highlighting that the best performance is reached for the injection locking conditions. (c) Total system consistency as a function of PR = P_{inj}/P_{VCSEL}. (d) Dimensionality of the system with the VCSEL ON and OFF for different input dimensionalities (bit-numbers). The VCSEL expands the dimensionality of the input highlighting the non-linearity of the device. Reproduced with permission from [37].

In addition, in [37] the authors link consistency, i.e. the ability of the system to respond in the same way when subjected to the same input, and dimensionality (numbers of degrees of freedom of the system) to the physical parameters λ_{inj}, PR, and I_{bias}. Figure 5(c) shows the clear dependence of consistency on optical injection power, the total system consistency saturates and reaches an excellent level above 99.5%.

In the same paper, a general way to gauge a system's dimensionality was proposed. The same random input sequence is injected into the LA-VCSEL, and the response of every neuron is recorded. The method relies on principal component analysis for noisy systems [42,43], and can generally be applied to other hardware ANNs. In Fig. 5(d), the dimensionality is measured for sequences of headers with the LA-VCSEL switched off as well as with the LA-VCSEL switched on. It is clear that the LA-VCSEL significantly increases the dimensionality of data representation. However, one has to say that rather than viewing the obtained dimensionality as absolute values, one should use their relative variation in direct comparisons, such as here to demonstrate the clear benefit of the LA-VCSEL on the PNN's capability to expand the dimensionality of data representation. This is due to approximations made in [42,43], which leverages slightly heuristic criteria for assigning principle components to noise.

5. Computing with spiking VCSEL neurons

A certain isomorphism between VCSELs and biological neurons has started to be explored. Here, we introduce VCSEL-based systems that are able to directly mimic (at ultrafast rates) the spiking action potentials of biological neurons and use the resulting photonic spiking signals to process information.

Biological neurons are known to communicate using electrical action potentials which take the form of temporal spiking signals. These are created when a neuron is subject to a stimulation from an external source or by neighbouring neurons. Remarkably, the generation of optical excitable spiking signals has also been observed in VCSELs, at ultrafast sub-nanosecond rates, multiple orders of magnitude faster than the time-scales of biological neurons [17,18]. However, while the different nonlinear dynamical responses occurring in VCSELs, including excitability, have been widely reported in the literature, it is only in recent years that the link between the nonlinear effects in VCSELs and neuronal behaviour has been proposed [44–54] towards novel paradigms in neuromorphic spike-based photonic processing systems.

5.1. Reports of excitability and neuronal responses in VCSELs

A first experimental report outlining the use of VCSELs as artificial photonic neurons appeared as early as 2010 [44]. That work described the use of optically-induced polarisation switching in a 1550 nm VCSEL to trigger different types of nonlinear activation functions, reproducing the response of neurons to excitatory and inhibitory stimuli. In a subsequent report in 2012 [45], the link between the spiking dynamical responses triggered in VCSELs and those used to process information by neurons, was proposed. In that work, optical injection into the subsidiary (orthogonally-polarised) mode of a 1550 nm VCSEL induced polarisation switching. The authors investigated the polarization resolved dynamics of the stimulated VCSEL and showed responses reproducing different neuronal dynamics, such as phasic spiking (the activation of a single spike at the onset of a stimulation) and tonic spiking (the continuous firing of excitable spikes in response to an extended stimulation). This was the first implementation of a dynamically excited VCSEL-neuron yielding neural-like responses at sub-ns time-scales, a method that was further theorised in [46] to explore the possibility of triggering excitable spiking responses in a VCSEL operating at the key telecom wavelength of 1550 nm. It was found that around the injection locking boundary (for both parallel and orthogonally-polarised optical injection), different excitable responses could be activated. Like in biological neurons excitable spikes had an activation threshold requirement, therefore revealing an experimental method of implementing controllable artificial VCSEL-based spiking neurons. The system was subsequently realised experimentally [18], demonstrating that excitable neuron-like spiking dynamics could indeed be triggered in a 1550 nm-VCSEL with precise control. As theorized, short 0.5 ns input stimulations successfully triggered 100 ps-long spikes using both orthogonal and parallel polarized optical injection, revealing also a high reproducibility of the spiking outputs. The precise control of neuron-like excitability was also demonstrated through the manipulation of the injection modulation. It was shown that increasing the duration of the stimulation triggered the continuous firing of tonic spikes. In subsequent experimental reports, the authors reported also the achievement of spike inhibitory behaviour [47], communication of excitable spikes between coupled VCSEL-neurons [48,49] and their potentials for photonic spike memory operation and for the emulation of retinal neuronal circuits [50].

Excitable pulses have also been observed in short-wavelength VCSELs under phase-modulated optical injection. M. Turconi et al. [51] reported excitable pulses in a 980 nm VCSEL around the injection locking boundary when adding 100 ps-long phase jumps of different amplitudes in the optically injected signals. Fig. 6 (a) shows the shape and efficiency of the phase-triggered excitable responses. Again, the excitable pulses required inputs to exceed an activation threshold for successful and consistent firing. The authors also showed that strong pulses in bias current could also trigger excitable responses from the VCSEL. The electrically-triggered spiking responses, however, were found to be less reliable and longer (typically 1 ns in duration) than those produced by optical injection with phase modulation. The activation of excitable spikes using the modulation of VCSEL bias current was again later demonstrated experimentally using VCSELs subject to intensity modulated optical injection [52]. Using phase-modulation, Garbin

et al. [53] also reported the regeneration of excitable optical spikes in a short-wavelength VCSEL under delayed optical feedback towards photonic spike memory operation. More recently, experimental and theoretical results successfully demonstrated resonator and integrator behaviour in phase modulated VCSEL systems producing multipulse excitability [54].
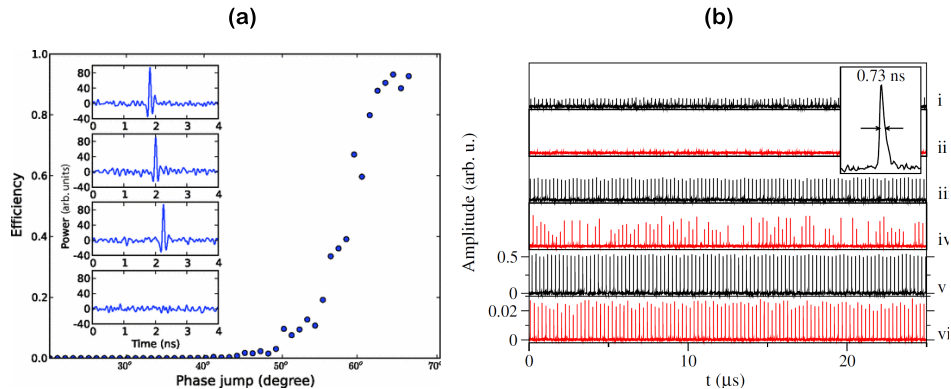

Fig. 6. Excitable spiking responses activated by (a) phase jump modulations in an injection locked VCSEL [51] and (b) optical pump modulations in a near threshold VCSEL-SA [17]. (a) The efficiency curve for excitable responses is plotted with respect to injection phase jump amplitude. The insets show individual excitable responses for phase jumps of 66°(top), 55°, and 52°for successful (third) and unsuccessful (bottom) cases. (b) Time series show the consistency of 100 excitable responses (red) to input pulses (black) of 0.4 (i,ii), 1.0 (iii,iv) and 1.78 (v,vi) input strength (scaled to the excitable threshold). The inset shows a 730 ps excitable response from the VCSEL-SA in series vi. (a) Reprinted with permission from [51] © 2022 The American Physical Society. (b) Reprinted with permission from [17] © The Optical Society.

In parallel, excitable spiking signals have also been investigated in VCSELs containing intracavity saturable absorbers (SA). We refer to these devices from now onwards as VCSEL-SAs. Work led by Barbay et al. [17] has focused experimentally on spiking micro-pillar VCSEL-SA systems, demonstrating that optically-pumped micropillar VCSEL-SAs (with emission at 980 nm when optically pumped at 800 nm) exhibited self-pulsating (spiking) regimes immediately after their lasing threshold. Barbay et al. also demonstrated the activation of 730 ps-long excitable spikes under optical pump modulation (Fig. 6 b), and the existence of a spike activation threshold. In addition, this team also reported neuronal processing features in spiking micropillar VCSEL-SA structures, including spike firing latency, refractoriness and integration of multiple inputs prior to spike firing [55–57]. These spiking behaviours were further confirmed by numerical simulations using the Yamada model for a semiconductor laser with a SA region. Numerical work by these authors also outlined the potentials of networks of evanescently coupled micropillar VCSEL-SAs to perform temporal spike logic operations (e.g. OR, AND) [58].

The activation of neuronal dynamics in VCSELs have also seen significant theoretical investigation via the SFM and Yamada models [59,26]. In addition to numerical work carried out by the teams at Strathclyde [18,47], Nice [54] and Paris [17,57,58], other groups also started to investigate numerically the spiking properties of VCSEL-neurons. In 2016, S. Xiang et al. [60] reported numerical results based on the SFM, validating the early 2012 experimental results of [45], and later expanded on that experimental work to widely report theoretically on the potentials of dynamical polarisation switching responses in VCSELs for high-speed neuronal-like functionalities [61]. In addition, a great body of theoretical work has recently appeared in literature focusing on optical spiking neurons based upon VCSEL-SAs [62–73]. An early theoretical

work [62] used a two-section rate-equation model to describe a VCSEL-SA and demonstrate numerically that excitable pulses could be activated in these devices under the injection of short optical pulses. This work also revealed that VCSEL-SAs could theoretically operate as a leaky integrate-and-fire (LIF) neurons, and operate in different interconnected architectures with brain-inspired connectivity. Multiple other theoretical works further investigated the spiking responses in VCSEL-SAs and their potential for a wide diversity of tasks and procedures, ranging from spiking convolutional neural networks for image processing [63], to spiking information encoding and storage [64–67], Sudoku solvers [74], unsupervised learning procedures based on Spike-Timing Dependent Plasticity (STDP) [68–70], spike pattern recognition [71,72], spiking XOR gate implementations [73], amongst others.

5.2. Spike-based processing systems with VCSELs

It is only very recently that the first experimental demonstrators of spike processing systems, with VCSEL neurons for ultrafast neuromorphic photonic computing, have started to emerge [75–80]. Using VCSEL spiking neurons, several processing tasks, typical of artificial intelligence (AI) implementations, have been reported (e.g. image processing, and temporal pattern recognition) with the desired advantages of ultrafast processing times and low energy usage. In 2020, Robertson et al. [75] demonstrated experimentally a method of classifying 4-bit digital patterns using a single VCSEL-neuron. In that work, as shown in Fig. 7 a, 4-bit patterns (with a bit rate of ~150 ps) were injected optically into a VCSEL-neuron which fired fast 100 ps spikes only in response to target patterns, remaining quiescent otherwise. In the same work [75], the authors used the leaky integrate-and-fire nature of a VCSEL-neuron to demonstrate experimentally a coincidence detection task, permitting the system to recognise the arrival of two different inputs within a very short temporal window (<420 ps). Similarly, all-optical XOR classification has been demonstrated on binary patterns, emulating pyramidal neurons, using an optical injection system subject to dual modulation [76].

More recently, spiking VCSEL-neurons have also been applied for image processing. Experimental demonstrations of image edge-feature detection [77] and binary convolution (that calculates the intensity gradients in images) [78] with spiking VCSEL neurons have been reported. Notably, these different functionalities were achieved at high processing rates (with GHz's input data signals) and low input power levels (tens of μWs), using hardware friendly systems and commercially available VCSELs. The latter reacted by triggering spikes (100 ps long) for image-pixels where specific features were detected, as shown in Fig. 7 b for the logo of the University of Strathclyde's Institute of Photonics. Recent work by Robertson et al. [79] has also shown that a single VCSEL-neuron can implement a full neuronal layer, performing image edge detection with reduced pre-processing requirements. Here, the Hadamard products of the target kernel with the image pixels is encoded into bursts of input pulses, which are subsequently integrated by the VCSEL-neuron, realising optical spiking convolution and edge detection. Additionally, this report demonstrated that the experimental photonic VCSEL layer could be combined with a software-implemented Spiking Neural Network (SNN). This hybrid VCSEL and software-implemented SNN demonstrated the accurate classification (>97% precision) of complex images from the MNIST hand-written digit image database. These works showed spike processing rate of 1.5 ns/pixel using a single commercially-sourced VCSEL without any specific device design optimisation. Higher processing speeds and more complex functionalities are expected for bespoke device designs and systems using multiple VCSEL neurons simultaneously.

Additionally, recent work by Hejda et al. [80] demonstrated experimentally the capability of spiking VCSEL-neurons to act as spike information encoders, using different spike coding mechanism, such as precise spike timing and spike rate encoding. Hejda et al. demonstrated experimentally that VCSEL-neurons, like their biological counterparts, show a spike latency and inter-spike refractory period that is dependent on input stimulation amplitude. This was used to
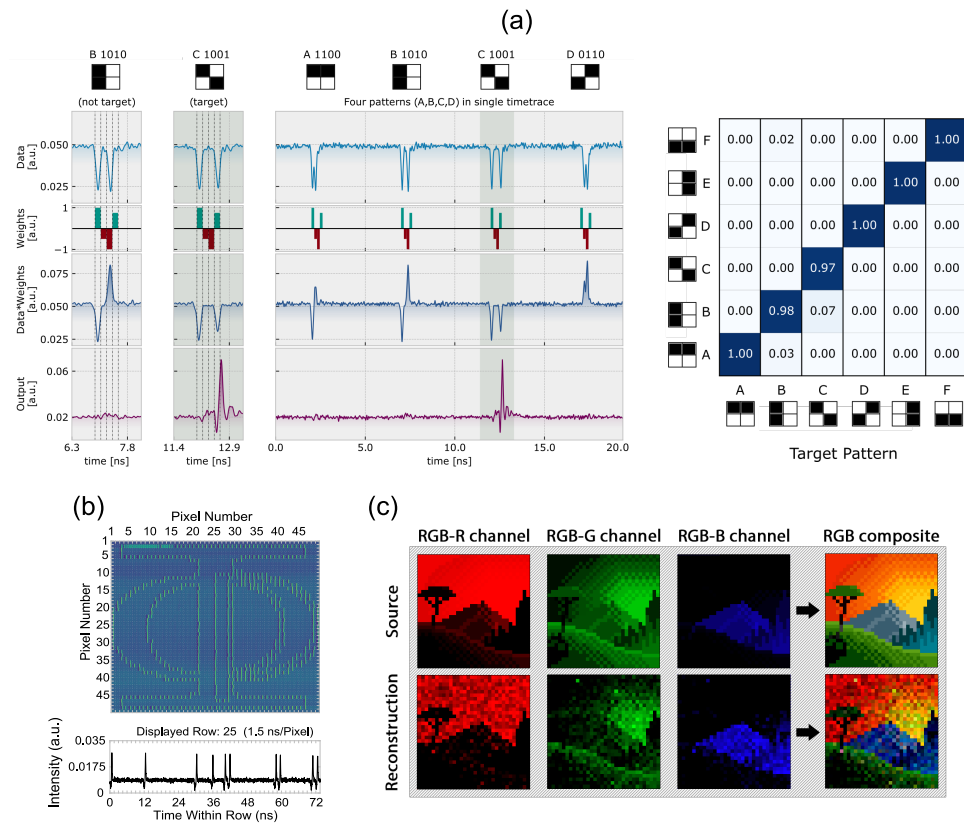
Fig. 7. Experimentally realised applications of excitable spiking VCSELs. (a) Fast (100 ps) input patterns are time division mulitplexed, weighted and injected into a VCSEL-neuron. Only the target input pattern results in the activation of an excitable response (a successful recognition). The confusion matrix reveals the recognition efficiency of various target patterns [75]. (b) Gradient-based edge detection of a black and white image (50x50 pixel Institute of Photonics logo) via convolution with a combination of vertical and horizontal kernels. Excitable VCSEL responses (bottom) corresponds to row 25 of the image, revealing the activation 10 excitable spikes [77]. (c) The fast (nanosecond rate) encoding and decoding of a RGB colour image into a spiking signal with variable spiking frequency. The RGB source image is compared the with spiking reconstruction after spike frequency analysis [81]. (b) Reprinted with permission from [77] © The Optical Society. (a) & (c) Reprinted with permission from [75,81], under the terms of the Creative Commons CC BY license.

implement precise spike-timing encoding of digital signals (digital to spiking format conversion) at rates over 1 Gbps, and spike rate encoding, where the amplitude of an strong (weak) input stimulus yielded faster (slower) spike firing frequencies. In a subsequent work, Hejda et al. [81] capitalised on the biologically-inspired rated coding ability of VCSEL-neurons, to demonstrate fast (nanosecond rate) encoding of image colour information for image processing functionalities (Fig. 7 c).

Artificial VCSEL-based optical neurons therefore provide exciting platforms towards fast (GHz rates) and low-energy neuromorphic photonic spike-processing systems. With access to threshold-and-fire and integrate-and-fire functionality, spiking VCSEL-neurons could be integrated into large interconnected photonic SNNs architectures for the implementation of complex light-enabled spike-based processing functionalities (e.g. image processing, computer vision, pattern recognition, etc.). VCSELs thus provide a consistent, all-optical, low power, and hardware friendly solution towards future ultrafast neuromorphic computing systems for AI technologies.

6. VCSEL and microlaser fabrication

The novel computing concepts discussed in this review rely crucially on vertically emitting lasers. VCSELs emit normal to the chip surface, can be controlled electrically, show high-speed dynamics and are energy efficient [82] and are much more compact than edge emitting lasers. In this regard, micropillar lasers are of high interest [83]. These nanophotonic structures with diameters in the few-μm range allow for the realization of photonic reservoirs consisting of hundreds or even thousands of small-scale lasers which can be coupled via external optical elements or integrated photonic structures. In addition to the small size footprint, microlasers offer the additional advantage that they operate in the regime of cavity quantum electrodynamics (cQED) which can reduce the threshold pump powers by orders of magnitude compared to conventional VCSELs to significantly improve the energy efficiency [84,85]. Beyond that, quantum dot - micropillars can also act as bright electrically driven single-photon emitters [86,87] which provides exciting opportunities towards quantum neural networks. In the following technological aspects and the fabrication of VCSELs, microlasers and single photon emitters for applications in photonic neuromorphic computing are discussed.

6.1. VCSEL fabrication

The fabrication of VCSELs requires multiple nanoprocessing steps. It starts with the epitaxial growth of a planar microresonator structure by means of molecular beam epitaxy (MBE) or metal-organic chemical vapour deposition (MOCVD). As schematically shown in Fig. 2 the microresonator is usually composed of a lower n-doped distributed Bragg reflector (DBR), the central cavity layer which is at least a $\lambda/2$ thick and includes the active area, and the upper p-doped DBR [7]. In the often used GaAs material system, the DBRs consists of typically more than 20 $\lambda/4$-thick AlGaAs/GaAs layers and the active medium in the central GaAs cavity is usually based on multiple InGaAs quantum wells located at the antinode of the confined light field [82]. In addition, the central cavity includes at least one thin AlGaAs layer with high Al-content (>90%), which is later oxidized and acts as current window and leads to lateral light confinement governing the emission beam profile. The lateral nanoprocessing of VCSEL devices starts with the patterning of circular mesa structures with diameters in the range of 20 - 30 μm by means of UV lithography and plasma etching. Next, the current aperture with a well-defined inner diameter is formed by wet thermal oxidation of the cavity-integrated AlGaAs layer. Finally, the lower n-contact and the upper ring-shaped p-contact are realized by additional UV lithography steps and metal deposition, leading to a VCSEL device as depicted in Fig. 2. It is noteworthy that especially in the case of long wavelength VCSELs, intracavity contacts are preferred to avoid optical losses due to free-carrier absorption in the doped DBRs [88].

Beyond individual VCSELs, which have are today standard components for optical data communication, VCSEL arrays have become more and more important in recent years, finding applications for example in face recognition in modern cell phones [89]. Moreover, they are highly attractive to implement photonic reservoir computing and schemes relying on fast optical matrix multiplication using 1D VCSEL arrays [90]. While VCSEL arrays are in principle commercially available, neuromorphic applications have specific requirements which demand the development of customized VCSEL arrays with special geometry and optical properties.

One example is a 5 x 5 VCSEL array optimized for photonic reservoir computing based on the diffractive coupling of VCSELs [14]. Generally, neuromorphic computing concepts require dense and spectrally homogenous VCSEL arrays, which in turn requires specific design and fabrication. One example of such an array is shown in Fig. 8(a). The 5×5 array includes 25 VCSELs with a pitch of only 80 μm, which is significantly smaller compared to commercial arrays. Dense packing facilitates efficient diffractive coupling within an available optical field of view [91]. Additionally, the wafer material was chosen to guarantee a high spectral homogeneity, which is essential to allow for locking all VCSELs to an external injection laser. As can be seen in Fig. 8(b), the emission wavelengths of the 25 VCSELs can be fine-tuned by the injection current of each individual emitter [9]. This enables a spectral homogeneity matching the injection locking range of 10-20 GHz. Moreover, due to a slight ellipticity of the emitters' cross-section, excellent polarization control of the 25 VCSELs is obtained with a standard deviation of only 1.5°.
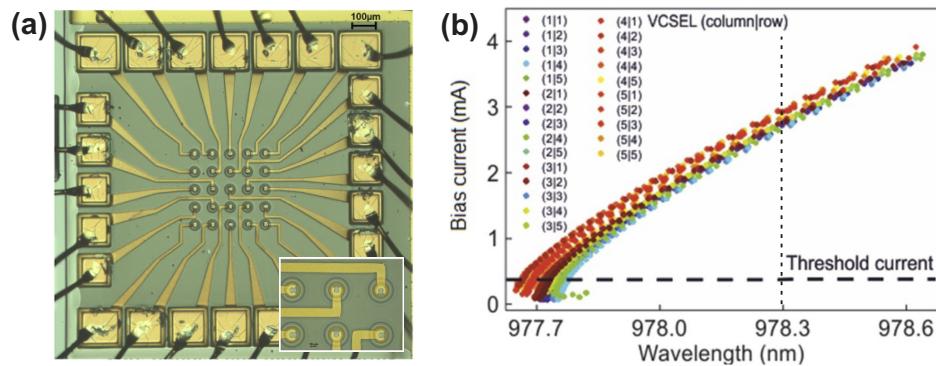

Fig. 8. (a) Optical microscope image of a compact 5 x 5 VCSEL array with a pitch of 80 μm. Each VCSEL is electrically contacted to allow for individual current injection and current-induced wavelength tuning. Inset: Zoom-in view of a subarray of 6 VCSELs. (b) Plot of the required injection currents to achieve a common target wavelength within the 5 x 5 VCSEL array. The dashed vertical line indicates that a common emission wavelength of 978.3 nm can be achieved by setting the injection currents of the individual emitters in a range of 2.6 - 3.0 μA. Reproduced with permission from Ref. [9]

6.2. High-β microlaser and dense microlaser arrays

Even VCSELs still pose limitations, not only in terms of the size-footprint, but also regarding the energy efficiency and modulation speed. To overcome such limitations, it is interesting to consider micro- and nanolasers which operate in the regime of cQED [92]. Here, small mode volumes and high cavity quality factors lead to enhanced light matter interaction which is quantified by the Purcell factor. The Purcell effect leads to a high fraction of spontaneous emission coupled into the lasing mode, which is described in terms of the β-factor and which leads to an order of magnitude reduction of the threshold pump power when comparing cavity-enhanced high-β micro- and nano-lasers with conventional semiconductor lasers [84]. Additionally, the tight mode

confinement in microlasers gives the opportunity to efficiently control the emission features such as the emission wavelength by the geometry of the laser cavity.

Micropillar lasers with quantum dot (QD) gain medium are a popular type of microlasers [83]. Alike to VCSEL devices, they emit vertically, and they can be driven electrically in a straightforward way [93]. In fact, large-scale micropillar arrays with small size footprint and high spectral homogeneity are ideally suited to realize the PRC proposed in Ref. [14]. To meet the requirements of this neuromorphic computing scheme the QD-micropillar array has to feature a small pitch below 10 μm and high spectral homogeneity on a scale of the injecting locking range of a few tens of GHz, i.e. the spectral homogeneity of the array must be better than about 200 μV.

In order to fulfill the said requirements, the microlaser-arrays have to be fabricated by state-of-the-art nanotechnology platforms. Similar to VCSEL devices QD-micropillar lasers are typically based on an epitaxial planar AlGaAs/GaAs microcavity structure with a lower and an upper DBR with up to 30 mirror pairs in an asymmetric design (3-4 more mirror pairs in the lower DBR to ensure directional emission via the upper DBR) and a central GaAs cavity, usually with a thickness of λ and a single layer of self-assembled InGaAs QDs at the field antinode for optical gain. Figure 9(a) shows a scanning electron microscopy (SEM) image of a QD-micropillar with a lower (upper) DBR composed of 27 and (23) $\lambda/4$-thick $Al_{0.9}Ga_{0.1}As$/GaAs mirror pairs [94]. The lower DBR is only partially (12 mirror pairs) etched, which is, however, sufficient to obtain the desired tight mode confinement, while maintaining a high Q-factor. Using electron beam lithography and plasma etching, dense arrays of such micropillar cavities can be realized with high accuracy. Figure 9(b) shows an excerpt of such an array consisting of 30 x 30 QD-micropillars with a pitch of 8.3 μm.

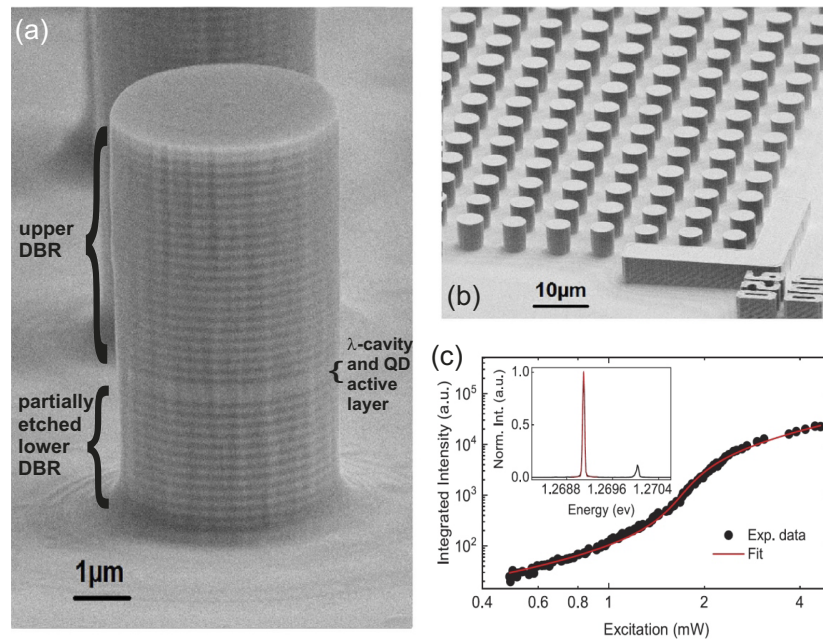**Fig. 9.** Dense QD-micropillar arrays for photonic reservoir computing. (a) SEM image of a QD-micropillar with a diameter of 5 μm. (b) SEM image of a dense arrays of QD micropillars with a pitch of 8.3 μm. (c) μPL emission spectrum (inset) and input-output characteristics of a 5 μm diameter micropillar with a β-factor of 2%. Reproduced with permission from Ref. [94].

An exemplary emission spectrum of an optically pumped QD-micropillar laser is depicted in the inset of Fig. 9(c). It is dominated by emission of the fundamental pillar mode HE_{11} at about 1.269 eV. The input-output dependence of the fundamental emission mode is plotted in Fig. 9(b) in double-logarithmic scale. The observed s-shaped behavior with a small non-linearity above the threshold pump power of about 1.8 mW is typical for cavity-enhanced microlasers. Fitting the experimental data with a rate-equations laser model allows us to extract a β-factor of 2%. Higher β-factors close to unity can be obtained for QD-micropillars with smaller diameter and adiabatic microcavity design.

Unfortunately, epitaxially grown micro-cavity wafers usually suffer from, both, a radial spectral dependence and local spectral inhomogeneities on a scale greater than what is acceptable for PRC. To address this issue and to reduce the spectral inhomogeneities of micropillar arrays advanced nanotechnology steps have to be applied for their fabrication. An interesting approach is "diameter tuning" which takes advantage of the tight mode confinement in micropillar cavities to precisely adjust the emission energy of each pillar in the array via its diameter during fabrication to compensate wafer inhomogeneities [94,95]. There, the emission energy of the respective microcavity area is first recorded with μm accuracy by micro-photoluminesence (μPL) mapping relative to alignment markers (see lower right corner in Fig. 9(b) for such a marker structure). With the knowledge of the local emission energy, the diameter of each micropillar is calculated where small (large) pillar diameters blue (red) shift its emission energy towards the target emission energy to compensate the spectral inhomogeneity of the underlying microcavity. As a result, after electron beam lithography and plasma etching, the spectral spread of emission energy of the micropillars in the fabricated arrays can be reduced from 1 meV to values as low as 120 μeV [94]. These results is very promising and further enhancement of the spectral homogeneity of large scale QD-micropillar arrays is expected by improved growth and nanoprocessing capabilities.

7. Outlook

The application of standard and more advanced VCSELs in various neuromorphic computing concepts and schemes is by now an established approach, with clearly identified merits and future possibilities. Similar to other areas in neuromorphic photonics, the crucial future steps are now an increasingly seamless interfacing and integration with other techniques in order to form complete computing systems. Crucial aspects here are (i) photonic integration, and (ii) more or less autonomous operation demonstrating a clear benefit in a relevant performance metrics compared to other, and most importantly, to electronic neurmorphic computing concepts.

Electronic implementations of artificial neural networks will, in the foreseeable future, remain out of reach for their photonic counterparts, thus, further research is needed to overcome the fundamental challenges faced by photonic implementations in terms of feature size, scalability, programmability and efficient nonlinearities. However, it is equally clear that photonic communication has an immense advantage in bandwidth and latency due to parallelism and speed, which are fundamentally linked to the bosonic, charge and mass-less nature of photons. Photonics, therefore, provides a promising strategy to implement the linear operation associated with the propagation of information across a PNN. Indeed, the state (weight setting) of the PNN could be represented in the physical state of a system for instance in the crystallinity of a PCM synaptic cell [96], or in the diffractive properties of materials [97]. Neuromorphic photonic implementations may therefore benefit from improved energy efficiency via direct utilization of light-matter interaction for some parts of the computation process (such as signal weighting). Combined with *autonomous* components for the accumulation of input signals and their nonlinear transformation, neuromorphic architectures leveraging photonics have the potential to substantially improve today's NN hardware. Here, fast, efficient, compact, and reliable VCSELs can play a key role. In combination with scalable photonic interconnects [13], VCSELs have therefore the potential to induce a shift in technology that facilitates multiple performance breakthroughs, but particularly

with regards to energy consumption per neural network operation (e.g. multiply, accumulate and nonlinear transformation operations). Similar arguments are considered in the general pursuit of next-generation circuit integration [5] with the goal of unlocking attojoule energy levels for information processing operations. As the communication part of a NN scales of order $O(N^2)$, the same arguments in favor for attojoule optoelectronics bear even more weight for the future of PNNs.

Disclosures. The authors declare no conflicts of interest.

Data availability. No data were generated or analyzed in the presented research.

References

1. A. W. Lohmann, R. G. Dorsch, D. Mendlovic, C. Ferreira, and Z. Zalevsky, "Space-bandwidth product of optical signals and systems," J. Opt. Soc. Am. A **13**(3), 470 (1996).
2. N. H. Farhat, D. Psaltis, A. Prata, and E. Paek, "Optical implementation of the Hopfield model," Appl. Opt. **24**(10), 1469 (1985).
3. B. J. Shastri, A. N. Tait, T. Ferreira de Lima, W. H. P. Pernice, H. Bhaskaran, C. D. Wright, and P. R. Prucnal, "Photonics for artificial intelligence and neuromorphic computing," Nat. Photonics **15**(2), 102–114 (2021).
4. D. Psaltis, D. Brady, X.-G. Gu, and S. Lin, "Holography in artificial neural networks," Nature **343**(6256), 325–330 (1990).
5. D. A. Miller, "Attojoule optoelectronics for low-energy information processing and communications," J. Lightwave Technol. **35**(3), 346–396 (2017).
6. J. Feldmann, N. Youngblood, M. Karpov, H. Gehring, X. Li, M. Stappers, M. Le Gallo, X. Fu, A. Lukashchuk, A. S. Raja, J. Liu, C. D. Wright, A. Sebastian, T. J. Kippenberg, W. H. P. Pernice, and H. Bhaskaran, "Parallel convolutional processing using an integrated photonic tensor core," Nature **589**(7840), 52–58 (2021).
7. K. Liu, C. R. Ye, S. Khan, and V. J. Sorger, "Review and perspective on ultrafast wavelength-size electro-optic modulators," Laser and Photonics Reviews **9**(2), 172–194 (2015).
8. N. Haghighi and J. A. Lott, "Electrically parallel three-element 980 nm VCSEL arrays with ternary and binary bottom DBR mirror layers," Materials **14**(2), 397 (2021).
9. T. Heuser, M. Pflüger, I. Fischer, J. A. Lott, D. Brunner, and S. Reitzenstein, "Developing a photonic hardware platform for brain-inspired computing based on 5 × 5 VCSEL arrays," JPhys Photonics **2**(4), 044002 (2020).
10. M. Lindemann, G. Xu, T. Pusch, R. Michalzik, M. R. Hofmann, I. Žutić, and N. C. Gerhardt, "Ultrafast spin-lasers," Nature **568**(7751), 212–215 (2019).
11. M. Parto, W. Hayenga, A. Marandi, D. N. Christodoulides, and M. Khajavikhan, "Realizing spin Hamiltonians in nanoscale active photonic lattices," Nat. Mater. **19**(7), 725–731 (2020).
12. T. Wang, S.-Y. Ma, L. G. Wright, T. Onodera, B. Richard, and P. L. McMahon, "An optical neural network using less than 1 photon per multiplication," (2021). 2104.13467, http://arxiv.org/abs/2104.1346.
13. J. Moughames, X. Porte, M. Thiel, G. Ulliac, M. Jacquot, L. Larger, M. Kadic, and D. Brunner, "Three dimensional waveguide-interconnects for scalable integration of photonic neural networks," Optica **7**(6), 640–646 (2020).
14. D. Brunner and I. Fischer, "Reconfigurable semiconductor laser networks based on diffractive coupling," Opt. Lett. **40**(16), 3854 (2015).
15. X. Porte, A. Skalli, N. Haghighi, S. Reitzenstein, J. A. Lott, and D. Brunner, "A complete, parallel and autonomous photonic neural network in a semiconductor multimode laser," JPhys Photonics **3**(2), 024017 (2021).
16. J. Vatin, D. Rontani, and M. Sciamanna, "Experimental reservoir computing using VCSEL polarization dynamics," Opt. Express **27**(13), 18579 (2019).
17. S. Barbay, R. Kuszelewicz, and A. M. Yacomotti, "Excitability in a semiconductor laser with saturable absorber," Opt. Lett. **36**(23), 4476 (2011).
18. A. Hurtado and J. Javaloyes, "Controllable spiking patterns in long-wavelength vertical cavity surface emitting lasers for neuromorphic photonics systems," Appl. Phys. Lett. **107**(24), 241103 (2015).
19. E. C. Mos, J. J. H. B. Schleipen, and H. de Waardt, "Optical-mode neural network by use of the nonlinear response of a laser diode to external optical feedback," Appl. Opt. **36**(26), 6654 (1997).
20. H. Jaeger and H. Haas, "Harnessing nonlinearity: predicting chaotic systems and saving energy in wireless communication," Science **304**(5667), 78–80 (2004).
21. L. Appeltant, M. C. Soriano, G. V. D. Sande, J. Danckaert, S. Massar, J. Dambre, B. Schrauwen, C. R. Mirasso, I. Fischer, G. Van der Sande, J. Danckaert, S. Massar, J. Dambre, B. Schrauwen, C. R. Mirasso, and I. Fischer, "Information processing using a single dynamical node as complex system," Nat. Commun. **2**(1), 468 (2011).

22. G. Van der Sande, D. Brunner, and M. C. Soriano, "Advances in photonic reservoir computing," Nanophotonics **6**(3), 561–576 (2017).

23. P. R. Prucnal, B. J. Shastri, T. F. de Lima, M. A. Nahmias, and A. N. Tait, "Recent progress in semiconductor excitable lasers for photonic spike processing," Adv. Opt. Photonics **8**(2), 228 (2016).

24. A. N. Tait, T. F. de Lima, M. A. Nahmias, H. B. Miller, H.-T. Peng, B. J. Shastri, and P. R. Prucnal, "Silicon Photonic Modulator Neuron," Phys. Rev. Appl. **11**(6), 064043 (2019).

25. H. Li, P. Wolf, P. Moser, G. Larisch, J. A. Lott, and D. Bimberg, "Vertical-cavity surface-emitting lasers for optical interconnects," SPIE Newsroom **25**, 126103 (2014).

26. M. San Miguel, Q. Feng, and J. V. Moloney, "Light-polarization dynamics in surface-emitting semiconductor lasers," Phys. Rev. A **52**(2), 1728–1739 (1995).

27. J. Bueno, D. Brunner, M. Soriano, and I. Fischer, "Conditions for reservoir computing performance using semiconductor lasers with delayed optical feedback," Opt. Express **25**(3), 2401–2412 (2017).

28. Y. Paquot, F. Duport, A. Smerieri, J. Dambre, B. Schrauwen, M. Haelterman, and S. Massar, "Optoelectronic Reservoir Computing," Sci. Rep. **2**(1), 287 (2012).

29. J. Bueno, J. Robertson, M. Hejda, and A. Hurtado, "Comprehensive performance analysis of a vcsel-based photonic reservoir computer," IEEE Photonics Technol. Lett. **33**(16), 920–923 (2021).

30. L. Larger, M. C. Soriano, D. Brunner, L. Appeltant, J. M. Gutierrez, L. Pesquera, C. R. Mirasso, and I. Fischer, "Photonic information processing beyond Turing: an optoelectronic implementation of reservoir computing," Opt. Express **20**(3), 3241 (2012).

31. D. Brunner, M. C. Soriano, C. R. Mirasso, and I. Fischer, "Parallel photonic information processing at gigabyte per second data rates using transient states," Nat. Commun. **4**(1), 1364 (2013).

32. J. Vatin, D. Rontani, and M. Sciamanna, "Enhanced performance of a reservoir computer using polarization dynamics in VCSELs," Opt. Lett. **43**(18), 4497–4500 (2018).

33. X. X. Guo, S. Y. Xiang, Y. H. Zhang, L. Lin, A. J. Wen, and Y. Hao, "Polarization multiplexing reservoir computing based on a VCSEL with polarized optical feedback," IEEE J. Sel. Top. Quantum Electron. **26**(1), 1–9 (2019).

34. J. Vatin, D. Rontani, and M. Sciamanna, "Experimental realization of dual task processing with a photonic reservoir computer," APL Photonics **5**(8), 086105 (2020).

35. K. Harkhoe, G. Verschaffelt, and G. Van der Sande, "Neuro-inspired computing with Spin-VCSELs," Appl. Sci. **11**(9), 4232 (2021).

36. F. Duport, B. Schneider, A. Smerieri, M. Haelterman, and S. Massar, "All-optical reservoir computing," Opt. Express **20**(20), 22783 (2012).

37. A. Skalli, X. Porte, N. Haghighi, S. Reitzenstein, J. A. Lott, and D. Brunner, "Computational measures of an injection-locked large area semiconductor laser," submitted to Optical Materials Express (2022).

38. J. Bueno, S. Maktoobi, L. Froehly, I. Fischer, M. Jacquot, L. Larger, and D. Brunner, "Reinforcement learning in a large-scale photonic recurrent neural network," Optica **5**(6), 756–760 (2018).

39. L. Andreoli, X. Porte, S. Chrétien, M. Jacquot, L. Larger, and D. Brunner, "Boolean learning under noise-perturbations in hardware neural networks," Nanophotonics **9**(13), 4139–4147 (2020).

40. T. Ackemann, S. Barland, M. Cara, M. Giudici, and S. Balle, "Spatial structures and their control in injection locked broad-area VCSELs," in *Nonlinear Guided Waves and Their Applications*, p. WC4 (Optical Society of America, 1999).

41. T. Ackemann, S. Barland, M. Giudici, J. R. Tredicce, S. Balle, R. Jaeger, M. Grabherr, M. Miller, and K. J. Ebeling, "Patterns in Broad-Area Microcavities," phys. stat. sol. (b) **221**(1), 133–136 (2000).

42. E. R. Malinowski, "Theory of error in factor analysis," Anal. Chem. **49**(4), 606–612 (1977).

43. D. Turner, R. Knuteson, H. Revercomb, C. Lo, and R. Dedecker, "Noise reduction of Atmospheric Emitted Radiance Interferometer (AERI) observations using principal component analysis," Journal of Atmospheric and Oceanic Technology **23**(9), 1223–1238 (2006).

44. A. Hurtado, A. Quirce, A. Valle, L. Pesquera, and M. J. Adams, "Nonlinear dynamics induced by parallel and orthogonal optical injection in 1550 nm vertical-cavity surface-emitting lasers (VCSELs)," Opt. Express **18**(9), 9423–9428 (2010).

45. A. Hurtado, K. Schires, I. D. Henning, and M. J. Adams, "Investigation of vertical cavity surface emitting laser dynamics for neuromorphic photonic systems," Appl. Phys. Lett. **100**(10), 103703 (2012).

46. R. Al-Seyab, I. D. Henning, M. J. Adams, and A. Hurtado, "Controlled single- and multiple-pulse excitability in vcsels for novel spiking photonic neurons," *Conference Digest - IEEE International Semiconductor Laser Conference* pp. 165–166 (2014).

47. J. Robertson, T. Deng, J. Javaloyes, and A. Hurtado, "Controlled inhibition of spiking dynamics in VCSELs for neuromorphic photonics: theory and experiments," Opt. Lett. **42**(8), 1560–1563 (2017).

48. T. Deng, J. Robertson, and A. Hurtado, "Controlled propagation of spiking dynamics in vertical-cavity surface-emitting lasers: towards neuromorphic photonic networks," IEEE J. Sel. Top. Quantum Electron. **23**(6), 1–8 (2017).

49. T. Deng, J. Robertson, Z.-M. Wu, G.-Q. Xia, X.-D. Lin, X. Tang, Z.-J. Wang, and A. Hurtado, "Stable propagation of inhibited spiking dynamics in vertical-cavity surface-emitting lasers for neuromorphic photonic networks," IEEE Access **6**, 67951–67958 (2018).

50. J. Robertson, E. Wade, Y. Kopp, J. Bueno, and A. Hurtado, "Toward neuromorphic photonic networks of ultrafast spiking laser neurons," IEEE J. Sel. Top. Quantum Electron. **26**(1), 1–15 (2020).

51. M. Turconi, B. Garbin, M. R. Feyereisen, M. Giudici, and S. Barland, "Control of excitable pulses in an injection-locked semiconductor laser," Phys. Rev. E **88**(2), 022923 (2013).

52. J. Robertson, E. Wade, and A. Hurtado, "Electrically controlled neuron-like spiking regimes in vertical-cavity surface-emitting lasers at ultrafast rates," IEEE J. Sel. Top. Quantum Electron. **25**(6), 1–7 (2019).

53. B. Garbin, G. Tissoni, and S. Barland, "Excitable pulses and diffusion of localized states in a driven semiconductor laser with delay," Cybernetics and Physics **7**(3), 96–101 (2018).

54. A. Dolcemascolo, B. Garbin, B. Peyce, R. Veltz, and S. Barland, "Resonator neuron and triggering multipulse excitability in laser with injected signal," Phys. Rev. E **98**(6), 062211 (2018).

55. F. Selmi, R. Braive, G. Beaudoin, I. Sagnes, R. Kuszelewicz, and S. Barbay, "Relative refractory period in an excitable semiconductor laser," Phys. Rev. Lett. **112**(18), 183902 (2014).

56. F. Selmi, R. Braive, G. Beaudoin, I. Sagnes, R. Kuszelewicz, and S. Barbay, "Temporal summation in a neuromimetic micropillar laser," Opt. Lett. **40**(23), 5690–5693 (2015).

57. F. Selmi, R. Braive, G. Beaudoin, I. Sagnes, R. Kuszelewicz, T. Erneux, and S. Barbay, "Spike latency and response properties of an excitable micropillar laser," Phys. Rev. E **94**(4), 042219 (2016).

58. V. A. Pammi, K. Alfaro-Bittner, M. G. Clerc, and S. Barbay, "Photonic computing with single and coupled spiking micropillar lasers," IEEE J. Sel. Top. Quantum Electron. **26**(1), 1–7 (2019).

59. M. Yamada, "A theoretical analysis of self-sustained pulsation phenomena in narrow-stripe semiconductor lasers," IEEE J. Quantum Electron. **29**(5), 1330–1336 (1993).

60. S. Xiang, A. Wen, and W. Pan, "Emulation of Spiking Response and Spiking Frequency Property in VCSEL-Based Photonic Neuron," IEEE Photonics J. **8**(5), 1–9 (2016).

61. S. Y. Xiang, H. Zhang, X. X. Guo, J. F. Li, A. J. Wen, W. Pan, and Y. Hao, "Cascadable Neuron-Like Spiking Dynamics in Coupled VCSELs Subject to Orthogonally Polarized Optical Pulse Injection," IEEE J. Sel. Top. Quantum Electron. **23**(6), 1–7 (2017).

62. M. A. Nahmias, B. J. Shastri, A. N. Tait, and P. R. Prucnal, "A Leaky Integrate-and-Fire Laser Neuron for Ultrafast Cognitive Computing," IEEE J. Sel. Top. Quantum Electron. **19**(5), 1–12 (2013).

63. M. Skontranis, G. Sarantoglou, S. Deligiannidis, A. Bogris, and C. Mesaritakis, "Time-Multiplexed Spiking Convolutional Neural Network Based on VCSELs for Unsupervised Image Classification," Appl. Sci. **11**(4), 1383 (2021).

64. Y. Zhang, S. Xiang, J. Gong, X. Guo, A. Wen, and Y. Hao, "Spike encoding and storage properties in mutually coupled vertical-cavity surface-emitting lasers subject to optical pulse injection," Appl. Opt. **57**(7), 1731 (2018).

65. S. Xiang, Y. Zhang, X. Guo, A. Wen, and Y. Hao, "Photonic Generation of Neuron-Like Dynamics Using VCSELs Subject to Double Polarized Optical Injection," J. Lightwave Technol. **36**(19), 4227–4234 (2018).

66. Y. Zhang, S. Xiang, X. Guo, A. Wen, and Y. Hao, "Polarization-resolved and polarization- multiplexed spike encoding properties in photonic neuron based on VCSEL-SA," Sci. Rep. **8**, 1–9 (2018).

67. Z. Zhang, Z. Wu, D. Lu, G. Xia, and T. Deng, "Controllable spiking dynamics in cascaded VCSEL-SA photonic neurons," Nonlinear Dyn. **99**(2), 1103–1114 (2020).

68. S. Xiang, J. Gong, Y. Zhang, X. Guo, Y. Han, A. Wen, and Y. Hao, "Numerical Implementation of Wavelength-Dependent Photonic Spike Timing Dependent Plasticity Based on VCSOA," IEEE J. Quantum Electron. **54**(6), 1–7 (2018).

69. S. Xiang, Y. Zhang, J. Gong, X. Guo, L. Lin, and Y. Hao, "STDP-based unsupervised spike pattern learning in a photonic spiking neural network with VCSELs and VCSOAs," IEEE J. Sel. Top. Quantum Electron. **25**(6), 1–9 (2019).

70. Z. Song, S. Xiang, Z. Ren, G. Han, and Y. Hao, "Spike sequence learning in a photonic spiking neural network consisting of VCSELs-SA with supervised training," IEEE J. Sel. Top. Quantum Electron. **26**(5), 1–9 (2020).

71. Y. Zhang, S. Xiang, X. Guo, A. Wen, and Y. Hao, "The Winner-Take-All Mechanism for All-Optical Systems of Pattern Recognition and Max-Pooling Operation," J. Lightwave Technol. **38**(18), 5071–5077 (2020).

72. S. Xiang, Z. Ren, Z. Song, Y. Zhang, X. Guo, G. Han, and Y. Hao, "Computing Primitive of Fully VCSEL-Based All-Optical Spiking Neural Network for Supervised Learning and Pattern Classification," IEEE Trans. Neural Netw. Learning Syst. **32**(6), 2494–2505 (2021).

73. S. Xiang, Z. Ren, Y. Zhang, Z. Song, and Y. Hao, "All-optical neuromorphic XOR operation with inhibitory dynamics of a single photonic spiking neuron based on a VCSEL-SA," Opt. Lett. **45**(5), 1104–1107 (2020).

74. S. Gao, S. Xiang, Z. Song, Y. Han, and Y. Hao, "All-optical Sudoku solver with photonic spiking neural network," Opt. Commun. **495**, 127068 (2021).

75. J. Robertson, M. Hejda, J. Bueno, and A. Hurtado, "Ultrafast optical integration and pattern classification for neuromorphic photonics based on spiking VCSEL neurons," Sci. Rep. **10**(1), 6098 (2020).

76. Y. Zhang, S. Xiang, X. Cao, S. Zhao, X. Guo, A. Wen, and Y. Hao, "Experimental demonstration of pyramidal neuron-like dynamics dominated by dendritic action potentials based on a VCSEL for all-optical XOR classification task," Photonics Res. **9**(6), 1055–1061 (2021).

77. J. Robertson, Y. Zhang, M. Hejda, J. Bueno, S. Xiang, and A. Hurtado, "Image edge detection with a photonic spiking VCSEL-neuron," Opt. Express **28**(25), 37526 (2020).

78. Y. Zhang, J. Robertson, S. Xiang, M. Hejda, J. Bueno, and A. Hurtado, "All-optical neuromorphic binary convolution with a spiking VCSEL neuron for image gradient magnitudes," Photonics Res. **9**(5), B201–B209 (2021).

79. J. Robertson, P. Kirkland, J. A. Alanis, M. Hejda, J. Bueno, G. D. Caterina, and A. Hurtado, "Ultrafast neuromorphic photonic image processing with a VCSEL neuron," arXiv 2110.01617, (2021).

80. M. Hejda, J. Robertson, J. Bueno, and A. Hurtado, "Spike-based information encoding in vertical cavity surface emitting lasers for neuromorphic photonic systems," JPhys Photonics **2**(4), 044001 (2020).

81. M. Hejda, J. Robertson, J. Bueno, J. A. Alanis, and A. Hurtado, "Neuromorphic encoding of image pixel data into rate-coded optical spike trains with a photonic VCSEL-neuron," APL Photonics **6**(6), 060802 (2021).

82. R. Michalzik, "VCSEL Fundamentals," in *Springer Series in Optical Sciences*, pp. 19–75 (Springer Berlin Heidelberg, 2012).

83. C. Gies and S. Reitzenstein, "Quantum dot micropillar lasers," Semicond. Sci. Technol. **34**(7), 073001 (2019).

84. G. Bjork and Y. Yamamoto, "Analysis of semiconductor microcavity lasers using rate equations," IEEE J. Quantum Electron. **27**(11), 2386–2396 (1991).

85. S. Reitzenstein, T. Heindel, C. Kistner, A. Rahimi-Iman, C. Schneider, S. Höfling, and A. Forchel, "Low threshold electrically pumped quantum dot-micropillar lasers," Appl. Phys. Lett. **93**(6), 061104 (2008).

86. T. Heindel, C. Schneider, M. Lermer, S. H. Kwon, T. Braun, S. Reitzenstein, S. Höfling, M. Kamp, and A. Forchel, "Electrically driven quantum dot-micropillar single photon source with 34% overall efficiency," Appl. Phys. Lett. **96**(1), 011107 (2010).

87. A. Schlehahn, A. Thoma, P. Munnelly, M. Kamp, S. Höfling, T. Heindel, C. Schneider, and S. Reitzenstein, "An electrically driven cavity-enhanced source of indistinguishable photons with 61% overall efficiency," APL Photonics **1**(1), 011301 (2016).

88. M. Mehta, D. Feezell, D. Buell, A. Jackson, L. Coldren, and J. Bowers, "Electrical design optimization of single-mode tunnel-junction-based long-wavelength VCSELs," IEEE J. Quantum Electron. **42**(7), 675–682 (2006).

89. A. Liu, P. Wolf, J. A. Lott, and D. Bimberg, "Vertical-cavity surface-emitting lasers for data communication and sensing," Photonics Res. **7**(2), 121 (2019).

90. R. Hamerly, L. Bernstein, A. Sludds, M. Soljačić, and D. Englund, "Large-scale optical neural networks based on photoelectric multiplication," Phys. Rev. X **9**(2), 021032 (2019).

91. S. Maktoobi, L. Froehly, L. Andreoli, X. Porte, M. Jacquot, L. Larger, and D. Brunner, "Diffractive coupling for photonic networks: how big can we go?" IEEE J. Sel. Top. Quantum Electron. **26**(1), 1–8 (2020).

92. W. W. Chow and S. Reitzenstein, "Quantum-optical influences in optoelectronics—an introduction," Appl. Phys. Rev. **5**(4), 041302 (2018).

93. C. Böckler, S. Reitzenstein, C. Kistner, R. Debusmann, A. Löffler, T. Kida, S. Höfling, A. Forchel, L. Grenouillet, J. Claudon, and J. M. Gérard, "Electrically driven high-Q quantum dot-micropillar cavities," Appl. Phys. Lett. **92**(9), 091107 (2008).

94. T. Heuser, J. Grose, S. Holzinger, M. M. Sommer, and S. Reitzenstein, "Development of highly homogenous quantum dot micropillar arrays for optical reservoir computing," IEEE J. Sel. Top. Quantum Electron. **26**(1), 1–9 (2020).

95. T. Heuser, J. Große, A. Kaganskiy, D. Brunner, and S. Reitzenstein, "Fabrication of dense diameter-tuned quantum dot micropillar arrays for applications in photonic information processing," APL Photonics **3**(11), 116103 (2018).

96. J. Feldmann, N. Youngblood, C. D. Wright, H. Bhaskaran, and W. H. Pernice, "All-optical spiking neurosynaptic networks with self-learning capabilities," Nature **569**(7755), 208–214 (2019).

97. T. Zhou, X. Lin, J. Wu, Y. Chen, H. Xie, Y. Li, J. Fan, H. Wu, L. Fang, and Q. Dai, "Large-scale neuromorphic optoelectronic computing with a reconfigurable diffractive processing unit," Nat. Photonics **15**(5), 367–373 (2021).